Research Square

Preprints are preliminary reports that have not undergone peer review.
They should not be considered conclusive, used to inform clinical practice,
or referenced by the media as validated information.

Supremacy of Magnetic Behaviour in n-Heptane Based M Doped Barium Ferrite ($BaFe_2O_4$) Nanoparticles (M: Co, Ni and Mn)

Dilip R
Department of Physics, Sri Ramakrishna Mission Vidyalaya College of Arts and Science
Jayaprakash R (jayaprakash.rajan.2015@gmail.com)
Department of Physics, Sri Ramakrishna Mission Vidyalaya College of Arts and Science

Original Research Full Papers

Keywords: Barium ferrite, n-Heptane, Morphology, Saturation Magnetization

Posted Date: February 8th, 2021

DOI: https://doi.org/10.21203/rs.3.rs-191057/v1

License: This work is licensed under a Creative Commons Attribution 4.0 International License.
Read Full License

Version of Record: A version of this preprint was published at Journal of Inorganic and Organometallic Polymers and Materials on March 17th, 2021. See the published version at https://doi.org/10.1007/s10904-021-01963-w.

Abstract

The M doped $BaFe_2O_4$ (M- Co, Ni and Mn) nanoparticles were synthesized through auto combustion method by using n-heptane as a surfactant. And also the weight percentage (wt%) of metals such as cobalt, nickel and manganese (10 wt%, 8 wt% and 6 wt%) in $BaFe_2O_4$ was optimized. The prominent orientation (212) and (311) of M doped $BaFe_2O_4$ is confirmed from XRD especially in 10 wt% of respective metals. The addition of metal doped in barium ferrite specific vibration on 770 and 445 cm^{-1} in FTIR spectra indicated the formation of M doped $BaFe_2O_4$. The influence of n-heptane as a surfactant on morphological change occurred in different metal doped was visualized from FESEM and TEM images. The different morphologies such as spherical, hexagonal platelets and small rectangular bar shaped were observed only by the inclusion of barium ferrite at surfactant medium. The analysis of EDX spectrum reflected the atomic percentage of elemental presence in the samples of M doped barium ferrite. Magnetic properties of these samples were studied by VSM. It revealed that 28.41 emu/g saturation magnetization (Ms) with 1655.64 Oe coercivity (Hc) and also induced ferromagnetic behaviour. The variation of dielectric constant indicated from dielectric study.

1 Introduction

Spinel ferrite is one of the types of complex oxides having general formula MFe_2O_4, where M represents metal cation. The application of spinel ferrite is originated from particular properties like structural, magnetic and dielectric properties. The permeant magnetization of ferrite turns the attention of researchers towards the best utilization like supercapacitor, photocatalysis and sensor [1–3]. The spinel structure closely connected to magnetic properties and its general structure is AB_2O_4 form, where A is represented as divalent and B as trivalent cations. The occupation of elements in the respective position of tetrahedral sites and octahedral sites in the spinel structure is playing a significant role. Here, Ba^{2+} as A sites are tetrahedral and Fe^{3+} as B sites are octahedral coordinated by oxygen atoms [4]. They can be effectively adjusted by using divalent ions such as Co, Ni, Mn, Zn, Ti and Sr [5–7]. The cobalt, nickel, manganese and barium ferrites come under low-cost materials that have good magnetic and dielectric properties. Spinel ferrite has soft magnetic properties with high electrical resistivity. The other advantage of these materials is mainly due to its excellent chemical stability and high mechanical durability. These ferrites even promote some advantage for chemical resistance, electrical resistivity and strong magnetic field. There are several methods for synthesizing the magnetic spinel ferrite such as co-precipitation, sol-gel, auto-combustion method, electrochemical method, hydrothermal method and micro emulsion [8–13].

The preparation of M doped BaFe2O4 nanoparticles (M- Co, Ni and Mn) is done by auto-combustion method using n-Heptane as surfactant. The identification of best weight percentage of metals based on reducing the particle size and formation of good morphology is also reported. In this study, there are three different metals (M) have ferromagnetic behaviour along with iron and various atomic radius may impact on magnetic, dielectric properties was discussed. The role of surfactants is to control the size and morphology change of materials. The surfactants are split into three categories such as cationic, anionic

and non-ionic surfactants [14]. Especially, cationic surfactants are used for controlling the size and agglomeration of atoms. Few examples are cetyltrimethylammonium bromide (CTAB), n-Heptane, amine [15]. Here, n-heptane is used as a surfactant for all samples (0.08 M). The formation of M doped $BaFe_2O_4$ nanoparticles is confirmed from X-ray diffraction (XRD) and FT-IR spectrum. The different morphological changes have occurred while doping the metals in barium ferrite which is observed from SEM and TEM. The formation of different morphological changes like thin crystalline platelets, spherical and spindle shaped are identified. The elemental presence has been done in EDX analysis. The magnetic and dielectric properties of metal doped samples are observed in VSM and dielectric studies.

2 Experimental Method

The chemicals used for the preparation were of analytic grade of barium nitrate ($Ba(NO_3)_2.6H_2O$), cobalt nitrate ($Co(NO_3)_2.6H_2O$), nickel nitrate ($Ni(NO_3)_2.6H_2O$), manganese nitrate ($Mn(NO_3)_2.6H_2O$), n-heptane ($H_3C(CH_2)_5CH_3$), ferric nitrate ($Fe(NO_3)_3.9H_2O$) and urea ($CO(NH_2)_2$) as raw materials.

The Co doped $BaFe_2O_4$ nanoparticles were prepared by using the auto-combustion method. Barium nitrate (20 wt%), cobalt nitrate (10 wt%) and ferric nitrate (70 wt%) were dissolved in 50 ml of distilled water. Subsequently, 0.08 M of n-heptane was dissolved in 50 ml distilled water. Urea was taken as a 25% from the total weight dissolved in distilled water. These solutions were mixed together at constant stirring for 3 h. A colloid solution was formed and it was heated up to 150 ^{o} C until the self-combustion was ignited in room temperature. The brown as-burnt sample was obtained as yield which was calcinated at 900 ^{o} C [16]. The same preparation procedure was adopted for synthesis of Co doped $BaFe_2O_4$ samples using other two different weight percentage such as 8 and 6 wt% of cobalt. The samples were named as sample (a1) for 10 wt% of Co doped $BaFe_2O_4$, sample (a2) for 8 wt% of Co doped $BaFe_2O_4$ and sample (a3) for 6 wt% of Co doped $BaFe_2O_4$.

The same procedure was carried out for synthesis of nickel doped barium ferrite nanoparticles. Barium nitrate (20 wt%), nickel nitrate (10 wt%) and ferric nitrate (70 wt%) was dissolved in 50 ml of distilled water. Subsequently, 0.08 M of n-heptane was dissolved in 50 ml distilled water. Urea was taken as a 25% from the total weight dissolved in distilled water. The same method of preparation as mentioned above was executed for synthesis under different weight percentage of nickel (10, 8 and 6 wt%) in $BaFe_2O_4$. The samples were named as sample (b1) for 10 wt% of Ni doped $BaFe_2O_4$, sample (b2) for 8 wt% of Ni doped $BaFe_2O_4$ and sample (b3) for 6 wt% of Ni doped $BaFe_2O_4$.

The Mn doped $BaFe_2O_4$ nanoparticles were prepared by using the auto-combustion method. Barium nitrate (20 wt%), cobalt nitrate (10 wt%) and ferric nitrate (70 wt%) were dissolved in 50 ml of distilled water. The above-mentioned procedure was carried out for the synthesis of manganese doped barium ferrite nanoparticles under Mn as different weight percentage such as 10, 8 and 6 wt%. The samples were named as sample (c1) for 10 wt% of Mn doped $BaFe_2O_4$, sample (c2) for 8 wt% of Mn doped $BaFe_2O_4$ and sample (c3) for 6 wt% of Mn doped $BaFe_2O_4$.

3. Results And Discussion

3.1 X-ray Diffraction Analysis

Figure 1(a1-a3) shows the X-ray diffraction patterns of Co doped barium ferrite nanoparticles with three different weight percentages such as sample (a1), sample (a2) and sample (a3) using n-Heptane which is sintered at 900 ^{o} C. The XRD pattern of sample (a1) represents the miller indices such as (212), (511), (412), (311), (321), (411), (422), (332), (024) and (440). The main peak (212) and (311) indicates the formation of Co doped $BaFe_2O_4$ well matched with the standard JCPDS card no. 70-2468 and 22-1086 [17]. The respective miller indices are (212), (511), (412), (422), (331), (024), (440) of sample (a2). Similarly, the miller indices (212), (511), (412), (422), (024) for sample (a3) indicate the formation of $BaFe_2O_4$ (JCPDS card no. 70-2468) [18]. The miller indices of (311) is absent at of less wt% of cobalt. In sample (a3), (440) miller indices are not found due to further decreases of wt% of cobalt nitrate. The (311) main peak is not present for both sample (a2) and sample (a3) of cobalt ferrite phase, but this peak is present in sample (a1). This result clearly indicates that wt% of Co dopant alters the phase of barium ferrite nanoparticles as well as it is assured that optimum level of Co is needed to act as dopant. The average crystalline size is calculated as 32 nm of sample (a1) by using Debye-Scherrer's formula [19].

Figure 1(b1-b3) shows the powder X-ray diffraction patterns of Ni doped $BaFe_2O_4$ nanoparticles with three different wt% of Ni such as sample (b1), sample (b2) and sample (b3). The respective peaks which correspond to miller indices such as (212), (511), (412), (311), (422), (024) and (440) planes of nickel doped barium ferrite as per JCPDS 70-2468 and 86-2267 [20] are observed. The peak at (212) and (311) represents formation of nickel doped barium ferrite. The average crystalline size of sample (b1) is measured as 31 nm. In sample (b2), barium ferrite phase (212), (511), (412), (422), (024) and (440) are only found. The similar formation of barium ferrite miller indices such as (212), (511), (412), (422), (331), (024) and (440) are found in sample (b3). The (311) main peak for cobalt ferrite phase is not found in sample (b2) and sample (b3) due to the lower wt% percentage of cobalt in barium ferrite nanoparticles.

Figure 1(c1-c3) represents the powder X-ray diffraction patterns of Mn doped $BaFe_2O_4$ nanoparticles of sample (c1), sample (c2) and sample (c3). The reflection peaks are obtained as (212), (511), (412), (311), (321), (411), (422), (332), (024), (511) and (440) planes of sample (c1) as per JCPDS (70-2468 and 89-4836). The peak at (212) and (311) indicates the formation of manganese doped barium ferrite nanoparticles. The peaks apart from main peak such as (332) and (411) show the impurity presence as Mn_2O_3 [21]. The average crystalline size is calculated for the sample (c1) as 33 nm. The formation of barium ferrite miller indices such as (212), (511), (412), (422), (024) and (440) is found in sample (c2). The similar formation of barium ferrite with miller indices such as (212), (412), (332) and (024) is found in sample (c3). The (311) main peak for manganese ferrite phase is not found in sample (c2) and sample (c3) due to the lower wt% of manganese in barium ferrite nanoparticles.

3.2 FTIR Analysis

In this analysis, the FTIR spectra of Co has been taken from different weight percentages (10wt%, 8wt% and 6wt%) in barium ferrite nanoparticles. The spectra are recorded from 2000 to 400 cm^{-1} as shown in Fig. 2(a1-a3). The main vibration peaks are 445.40 cm^{-1}, 626.66 cm^{-1}, 773.76 cm^{-1}, 975.48 cm^{-1} and 1030.48 cm^{-1}. The strong vibrational band observed at 773.76 cm^{-1}, 626.66 cm^{-1} and 445.40 cm^{-1} indicate metal-oxygen vibration between Co-O, Ba-O and Fe-O. In sample (a2), the main peaks are observed as 434.59 cm^{-1}, 528.77 cm^{-1}, 830.53 cm^{-1} and 966.45 cm^{-1} which shows mostly the metallic vibrations [22]. The peaks at 430.51 cm^{-1}, 578.56 cm^{-1}, 862.36 cm^{-1} and 926.02 cm^{-1} are found. In samples (a2-a3) vibrational bands at 773 cm^{-1} for Ba-O are also observed. It is well matched with XRD pattern, because sample (a1) shows the Ba-O, Co-O and Fe-O vibrations as well as formation of Co doped $BaFe_2O_4$ exhibits in XRD. In samples (a2-a3) $BaFe_2O_4$ is only obtained, so it is well matched with XRD.

The Ni doped $BaFe_2O_4$ with different wt% of Ni is subjected to FTIR study and it is shown in Fig. 2(b1-b3). The assigned peak at 454.19 cm^{-1} for sample (b1), 448.60 cm^{-1} for sample (b2) and 443.44 cm^{-1} for sample (b3) are identified the metallic ions (Fe, Ni) vibrations. The peaks around 770 cm^{-1} and 1032 cm^{-1} represent the vibration of Ba-O found at sample (b1). In sample (b2-b3) there is a shift from 770 cm^{-1} to 765 cm^{-1} and 1032 cm^{-1} to 1248 cm^{-1}peaks. The respective changes are also observed in XRD pattern.

The FT-IR spectra of the prepared sample (c1), sample (c2) and sample (c3) are recorded and respective vibrations are shown in Fig. 2(c1-c3). The peaks are 452.04 cm^{-1}, 621.93 cm^{-1}, 772.47 cm^{-1} and 1046.45 cm^{-1} for sample (a1) which are strong vibrational band indicated the Ba-O, Mn-O and Fe-O ions. The absorption peak around 773.12 cm^{-1} and 1037.51 cm^{-1} in Fig. 2 represent the vibration of Ba-O [23]. The peaks around at 620 cm^{-1} and 445 cm^{-1} belong to the vibration of Fe-O as observed from the respective peaks. The curve (c2) indicates the Ba-O vibration at 771.32 cm^{-1} [24]. The similar vibration of 768.06 cm^{-1} appeared in sample (c3). The result exhibits phase deviation and is matched with XRD analysis.

3.3 FESEM Analysis

Field Emission Scanning Electron Microscope (FESEM) image of Co doped $BaFe_2O_4$ for n-Heptane as surfactants are shown in Fig. 3(a1). The XRD and FTIR study reveals that higher weight percentage of cobalt (10 wt%) has formed the respective Co doped $BaFe_2O_4$ nanoparticles. FESEM clearly shows the effect of surfactants over metal doped barium ferrite which forms thin platelets due to n-heptane as surfactant. The major formation of thin platelets is identified in the sample (a1). In sample (b1), the morphology changes from thin platelets to spherical and elongates sphere-shaped particles due to the role of n-heptane [25]. The morphology of Ni doped $BaFe_2O_4$ clearly shows the effect of surfactant to produce the specific change in morphology. Similarly, the spindle shaped morphology as major part is found in sample (c1) due to the effect of Mn as well as n-heptane surfactant in Mn-$BaFe_2O_4$ nanoparticle. The changes in metal doped $BaFe_2O_4$ caused for a morphological transition from thin platelets to spherical shaped particle along with spindle shape particles were identified.

3.4 EDX Analysis

The EDX spectrum of sample (a1), sample (b1) and sample (c1) of M doped barium ferrite nanoparticles clearly depicts the presence of elemental composition in each sample. The elemental composition in terms of atomic percentage and weight percentage is shown in Fig. 4(a1) which indicates the levels of elemental presence in Co doped $BaFe_2O_4$. It reveals the major presence of Ba, Fe, Co and O elements in the sample (a1). The atomic percentages of the elements are Ba as 6.42, Fe as 30.52, Co as 4.2, O as 59.12. The Fig. 4(b1) shows the elemental composition which are indicating the levels of elemental presence in Ni doped $BaFe_2O_4$. It reveals the major presence of Ba, Fe, Ni and O elements in the samples. The atomic percentages of the elements are Ba as 7.26, Fe as 29.15, Ni as 4.5, O as 59.39. Similarly, the elemental composition of Mn doped $BaFe_2O_4$ as shown in Fig. 4(c1). The atomic percentages of the elements are Ba as 7.56, Fe as 29.12, Mn as 3.79, O as 59.51 these values are maintained good stoichiometry.

3.5 TEM Analysis

Figure 5 shows the transmission electron microscope image of sample (a1), sample (b1) and sample (c1) of M doped barium ferrite (M: Co, Ni & Mn) nanoparticles. The TEM image exhibits in-depth magnification of the above-prepared samples. The shapes of nanoparticles are in slightly agglomerated state of sample (a1) and it shows that the spherical nanoparticles are stuck over the thin crystalline platelets and it is shown in the Fig. 5(a1). The elongated spherical shaped particles are observed in sample (b1). It is formed due to the effect of surfactant as n-heptane and Ni dopant as shown in Fig. 5(b1). Further, doping of next metal as manganese shows a deformation of thin platelets into spindle shape which coexists of hexagonal shaped particle, oval shaped particle and sphere. These shaped particles are clubbed together and formed spindle like structure. The formations of spindle like structure are shown in Fig. 5(c1). The image of 0.08 M of n-heptane in M doped barium ferrite nano-powder as created a significant change in morphology from the thin platelets, elongated spherical shape and spindle shaped particles [26]. The TEM image of sample (a1) gives the average length of the platelets that is 35 nm and breath of the platelet is 21 nm in Co doped $BaFe_2O_4$ nanoparticles. Similarly, the average diameter of spherical particles is around 39 nm for Ni doped $BaFe_2O_4$ nanoparticles (sample (b1)). The average diameter of the spherical shaped is appeared as 42 nm for Mn doped $BaFe_2O_4$ nanoparticles (sample (c1)). The insert fig. in Fig. 5(a1, b1 and c1) shows the selected area electron diffraction (SAED) patterns which indicate that the M doped $BaFe_2O_4$ nanoparticles are crystalline in nature. The diffraction planes of the corresponding main peaks as observed in the XRD are well matched with the concentric circles of the SAED pattern.

3.6 VSM Analysis

Magnetic properties of the prepared samples were analysed by vibrating sample magnetometer with maximum applied field of ± 15 kOe at room temperature. Hysteresis curves of M doped barium ferrite nanoparticles (M: Co, Ni and Mn) with n-heptane such as sample (a1), sample (b1) and sample (c1) are

shown in Fig. 6. The saturation magnetization of M doped barium ferrite depends on various parameters such as particle size, morphology of particle, magnetic anisotropy and components present in all samples. The obtained saturation magnetization (M_s) value of sample (a1) is 28.41 emu/g and its coercivity (H_c) value is 1655.64 Oe. Similarly, value of M_s is 26.29 emu/g and 25.41 emu/g for sample (b1) and sample (c1). H_c value of sample (b1) and sample (c1) is 2275.29 Oe and 1562.95 Oe respectively. The higher level of saturation magnetization attains in sample (a1) and maximum value of coercivity is obtained in sample (b1). Same weight percentage of different metals doped barium ferrite exhibits variation in Ms and Hc value due to the level of Ba^{2+} Co^{2+} Ni^{2+} Mn^{2+} is occupied by Fe^{2+} in the respective tetrahedral site. So, the well-defined formation of M doped $BaFe_2O_4$ in Co and Ni enriches the magnetic property [23]. This result reveals that the saturation magnetization is increased due to decrease in particle size. It also confirms that particle size creates a high impact on the saturation magnetization and coercivity values. The particle size leads to a change in morphology which is more responsible for the change in domain walls [27]. The domain walls are increasing according to different metals doped in barium ferrite nanoparticles. The saturation magnetization and coercivity value is inversely proportional to the particle size. Magnetic properties of M doped barium ferrite nanoparticles with n-heptane satisfy the proportionality between saturation magnetization and particle size. The sample (a1) exhibits maximum level of Ms value and higher level of Hc value is shown in sample (b1).

3.7 Dielectric study

The dielectric constant and dielectric loss is measured for the M doped barium ferrite nanoparticles with n-heptane such as sample (a1), sample (b1) and sample (c1) in the frequency range between 50Hz and 1MHz. The calculated dielectric constants for samples (a1-c1) show the decreasing trend on increase frequency in all doped levels of metals. Then it reaches the constant value at certain higher frequency. The variation in dielectric loss is also observed for the above-mentioned samples. The reverse behaviour of dielectric constant is observed on calculating dielectric loss. The curves are drawn between dielectric constant (ε) and log frequency (Hz) as shown in Fig. 7(a1-c1). The variation of dielectric constant for sample (a1) is from 116.54 to 6.7. Similarly, the dielectric constant variation is observed as 96.28 to 6.6 for the sample (b1) and 55.12 to 6.6 for the sample (c1). It clearly shows that the different metal has different level of dielectric constant. The maximum value of the dielectric constant is 116.54 for sample (a1). The similar behaviour is experienced at all ranges of frequency for the samples (a1-c1). According to Koop's, the decrease in dielectric constant in high frequency is observed due to the formation of well conducting grains, which is separated by the less conducting grain boundaries [28]. The variation of dielectric constant and dielectric loss is due to size and shape of barium ferrites. The observed change in the dielectric constant can be explained on the basis of hopping conduction between Fe^{3+} and Fe^{2+} pairs of ions [29]. High polarization dipoles are oriented at a low frequency range of these ions and the dielectric constant value reaches to an optimum value [30]. Similarly, the variation of dielectric loss (D) with respect to log frequency (Hz) is shown in Fig. 8.8 (a1-c1). The dielectric loss is predicted in the range of 4.82 to 0.18 for sample (a1), 4.42 to 0.20 for sample (b1) and 3.30 to 0.19 for sample (c1). This change also indicated the normal behaviour of ferrites.

4 Conclusion

The M doped barium ferrite nanoparticle (M: Co, Ni and Mn) with magnetic and morphological properties was obtained by using auto combustion process. The different dopants such as cobalt, nickel and manganese exhibited different particle size, morphology and saturation magnetization values. The particle size of M doped $BaFe_2O_4$ nanoparticles was changed according to atomic radius of different metals which acts as dopants. The good crystallinity was retained by M doped $BaFe_2O_4$ nanoparticles for all samples against XRD pattern. The shape of M doped barium ferrite nanoparticles formed thin platelets, spherical and spindle shape with low agglomeration for samples. The Co doped $BaFe_2O_4$ nanoparticles obtained higher saturation magnetization as 28.41 emu/g (Ms) and Ni doped $BaFe_2O_4$ nanoparticles obtained higher coercivity value (2275.49 Oe).

References

1. H. Kennaz et al., Synthesis and electrochemical investigation of spinel cobalt ferrite magnetic nanoparticles for supercapacitor application. J. Solid. State. Electr. **22**, 835–847 (2018)
2. A. Shabbir et al., Zirconium substituted spinel nano-ferrite Mg0. 2Co0. 8Fe2O4 particles and their hybrids with reduced graphene oxide for photocatalytic and other potential applications. Ceram. Int. **45**, 16121–16129 (2019)
3. Ch Srinivas et al., Study of magnetic behavior in co-precipitated Ni–Zn ferrite nanoparticles and their potential use for gas sensor applications. J. Magn. Magn. Mater. **502**, 166534 (2020)
4. N. Kannapiran et al., Poly (o-phenylenediamine)/NiCoFe2O4 nanocomposites: synthesis, characterization, magnetic and dielectric properties. J. Magn. Magn. Mater. **423**, 208–216 (2017)
5. M.L. Aparna et al., A comparative study on the supercapacitive behaviour of solvothermally prepared metal ferrite (MFe2O4, M = Fe, Co, Ni, Mn, Cu, Zn) nanoassemblies. J. Alloys Compd. **745**, 385–395 (2018)
6. R. Rathi, R. Neogi, Structural, electric and magnetic properties of titanium doped Ni-Cu-Zn ferrite. Mater. **3**, 2437–2442 (2016)
7. Z.K. Heiba, A.M. Wahba, M. Mohamed Bakr, Phase analysis and cation distribution correlated with magnetic properties of spinel Ba 1 – x Sr x Fe 2 O 4 ferrites prepared at different annealing temperatures. J. Mater. Sci.: Mater. Electron. **31**, 12482–12492 (2020)
8. R. Shahraki, Raeisi et al., Structural characterization and magnetic properties of superparamagnetic zinc ferrite nanoparticles synthesized by the coprecipitation method. J. Magn. Magn. Mater. **324**, 3762–3765 (2012)
9. S.E. Shirsath et al., Ferrites obtained by sol-gel method." Handbook of sol-gel science and technology. Springer Cham. 695–735 (2018)
10. A.S. Džunuzović et al., Structure and properties of Ni–Zn ferrite obtained by auto-combustion method. J. Magn. Magn. Mater. **374**, 245–251 (2015)

11. E. Mazarío et al., Synthesis and characterization of manganese ferrite nanoparticles obtained by electrochemical/chemical method. Mater. Des. **111**, 646–650 (2016)
12. G. Allaedini, S.M. Tasirin, P. Aminayi, Magnetic properties of cobalt ferrite synthesized by hydrothermal method. Int. Nano Lett. **5**, 183–186 (2015)
13. R. Ali et al., Impacts of Ni–Co substitution on the structural, magnetic and dielectric properties of magnesium nano-ferrites fabricated by micro-emulsion method. J. Alloys Compd. **584**, 363–368 (2014)
14. E. Foulani, A-H., et al. Effect of surfactants on the optical and magnetic properties of cobalt-zinc ferrite Co0. 5Zn0. 5Fe2O4. J. Alloys Compd. **774**, 1250–1259 (2019)
15. M. Das, Shyamal, Bououdina, C. Manoharan, The influence of cationic surfactant CTAB on optical, dielectric and magnetic properties of cobalt ferrite nanoparticles. Ceram. Int. **46**, 11705–11716 (2020)
16. J. Balavijayalakshmi, N. Suriyanarayanan, R. Jayapraksah, Influence of copper on the magnetic properties of cobalt ferrite nano particles. Mater. Lett. **81**, 52–54 (2012)
17. W. Zhang et al., A general approach for fabricating 3D MFe2O4 (M = Mn, Ni, Cu, Co)/graphitic carbon nitride covalently functionalized nitrogen-doped graphene nanocomposites as advanced anodes for lithium-ion batteries. Nano Energy. **57**, 48–56 (2019)
18. P. Shen et al., Effect of La-Ni substitution on structural, magnetic and microwave absorption properties of barium ferrite. Ceram. Int. **43**, 4846–4851 (2017)
19. P. Sangaiya, R. Jayaprakash, Influence of annealing temperature and electrical conductivity of α-Fe 2 O 3 nanoparticles for Schottky barrier diode. J. Mater. Sci.: Mater. **31**, 15153–15174 (2020)
20. K. Al Yaqoob et al., Selectivity and efficient Pb and Cd ions removal by magnetic MFe2O4 (M = Co, Ni, Cu and Zn) nanoparticles. Mater. Chem. Phys. **232**, 254–264 (2019)
21. A. Cetin, A.M. Önal, Emren Nalbant Esenturk. Nanowires assembled from iron manganite nanoparticles: Synthesis, characterization, and investigation of electrocatalytic properties for water oxidation reaction. Mater, 34, 3231–3239 (2019)
22. S.F. Wang, Q. Li, X.T. Zu, X. Xiang, W. Liu, S. Li, Phase controlled synthesis of (Mg, Ca, Ba)-ferrite magnetic nanopar- ticles with high uniformity. J Magn Magn Mater. **419**, 464–475 (2016)
23. E. Ranjith Kumar, R. Jayaprakash, J. Chandrasekaran, Effect of fuel ratio and the impact of annealing temperature on particle size, magnetic and dielectric properties of manganese substituted CuFe2O4 nanoparticles. Superlattice Microst. **64**, 343–353 (2013)
24. R. Peymanfar et al., Preparation and Identification of BaFe2O4 Nanoparticles by the Sol–Gel Route and Investigation of Its Microwave Absorption Characteristics at Ku-Band Frequency Using Silicone Rubber Medium. MDPI **2**, 17 (2018)
25. R. Dilip, R. Jayaprakash, Requisite of Surfactant (CTAB, n-Heptane, and Tri-sodium Citrate) Levels on Enhancement of Magnetic Property and Morphology Changes of Barium Ferrite (BaFe 2 O 4) Nanoparticles. J Supercond. Nov. Magn. **33**, 3799–3808 (2020)

26. L. Du et al., Surfactant-assisted solvothermal synthesis of Ba (CoTi) x Fe12 – 2 x O19 nanoparticles and enhancement in microwave absorption properties of polyaniline. J. Phys. Chem. C **114**, 19600–19606 (2010)
27. S.R. Kulkarni, C.M. Kanamadi, B.K. Chougule, Dielectric and magnetoelectric properties of (x) Ni0. 8Co0. 1Cu0. 1Fe2O4/(1 – x) PbZr0. 8Ti0. 2O3 composites. Mater. Res. Bull. **40**, 2064–2072 (2005)
28. A.M. Abdeen, Dielectric behaviour in Ni–Zn ferrites. J. Magn. Magn. Mater. **192**, 121 (1999)
29. N. Kannapiran et al., Poly (o-phenylenediamine)/NiCoFe2O4 nanocomposites: synthesis, characterization, magnetic and dielectric properties. J. Magn. Magn. Mater. **423**, 208–216 (2017)
30. E. Kumar, Ranjith et al., Effect of reaction time on particle size and dielectric properties of manganese substituted CoFe2O4 nanoparticles. J. Phys. Chem. Solids **74**, 110–114 (2013)

Figures

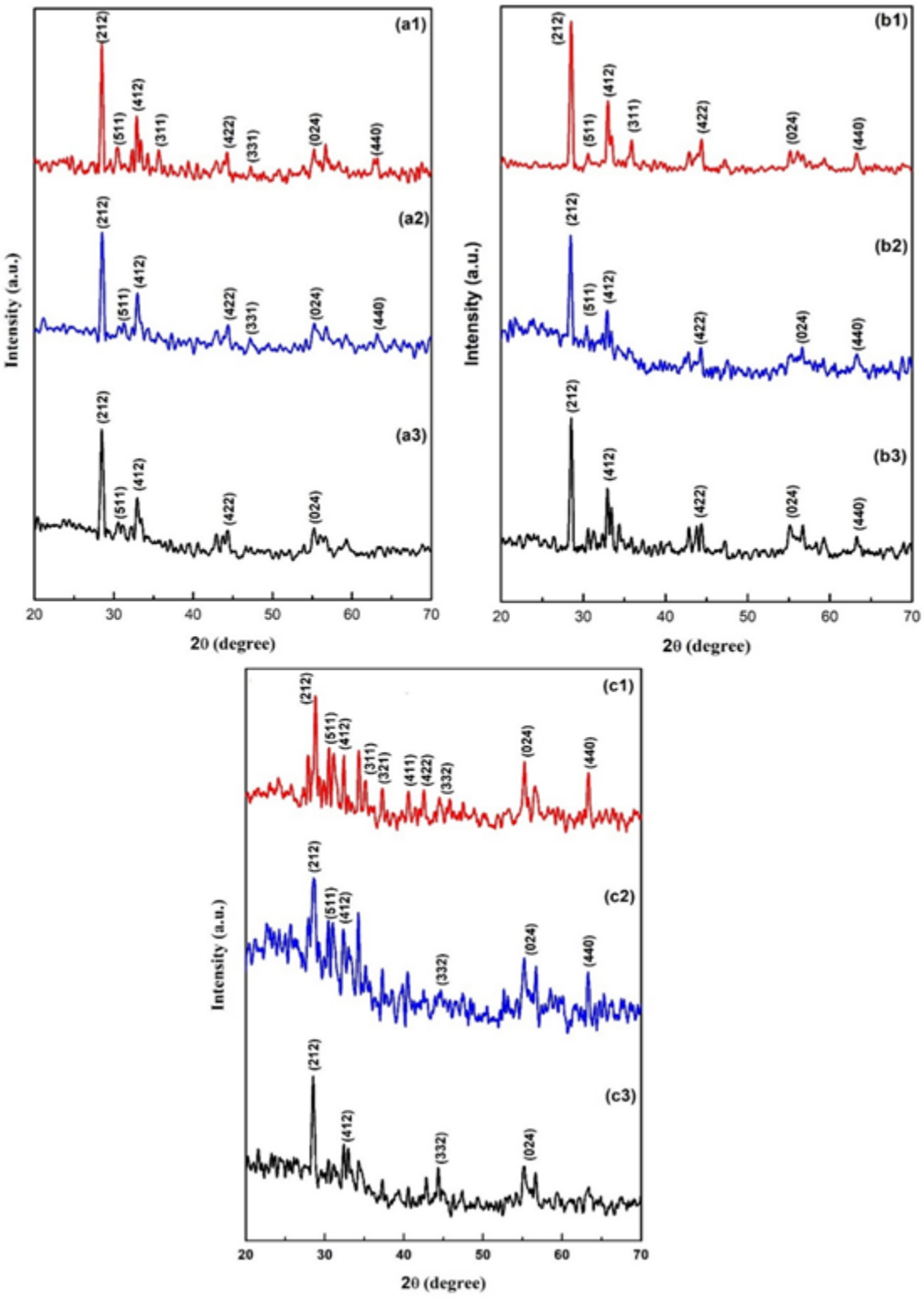

Figure 1

XRD pattern of M doped BaFe2O4 nanoparticles with different wt% (10, 8 and 6 wt%) such as (a1-a3) for Cobalt, (b1-b3) for Nickel and (c1-c3) for Manganese.

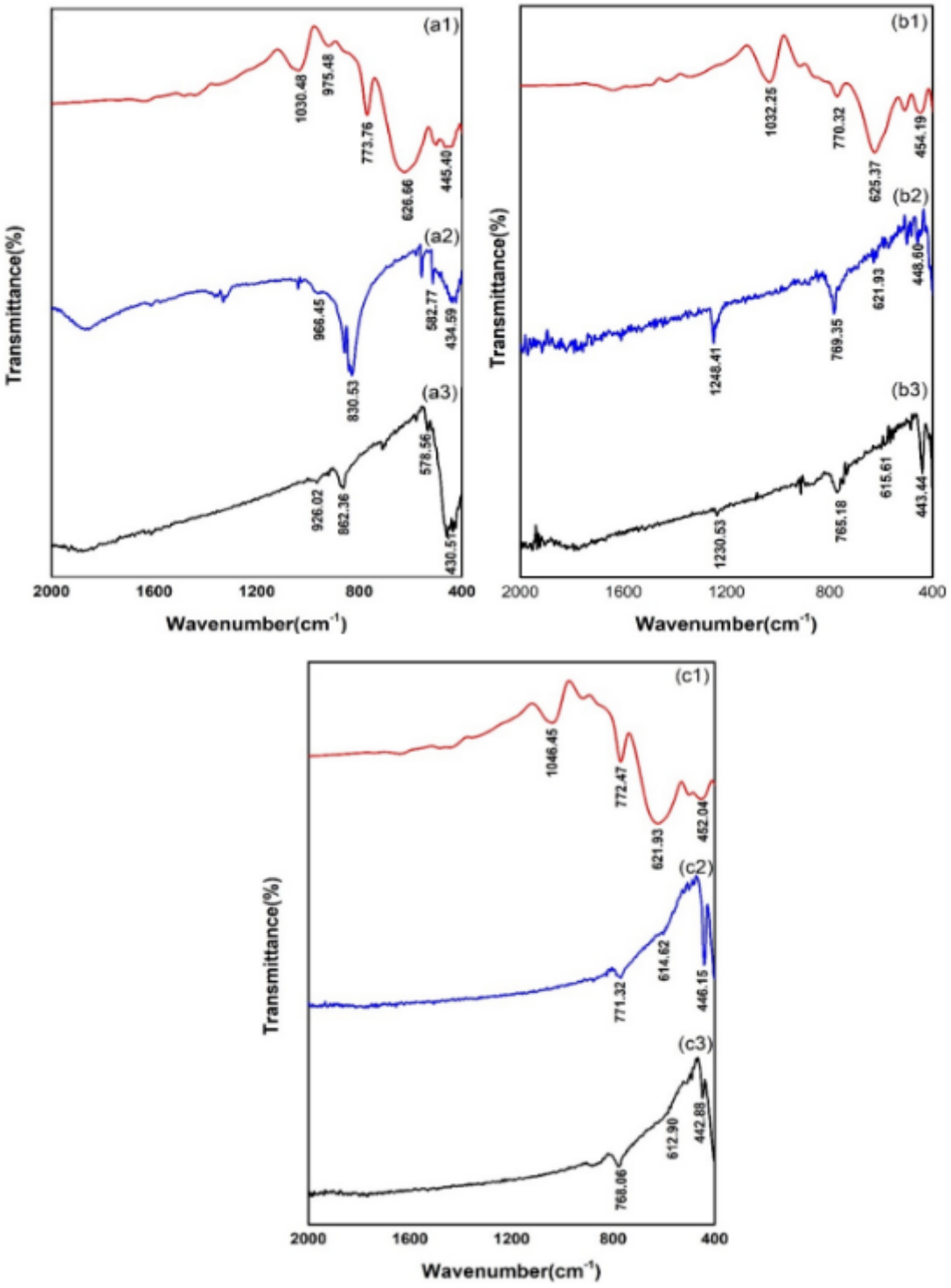

Figure 2

FTIR spectrum of M doped BaFe2O4 nanoparticles with different wt% (10, 8 and 6 wt%) such as (a1-a3) for Cobalt, (b1-b3) for Nickel and (c1-c3) for Manganese.

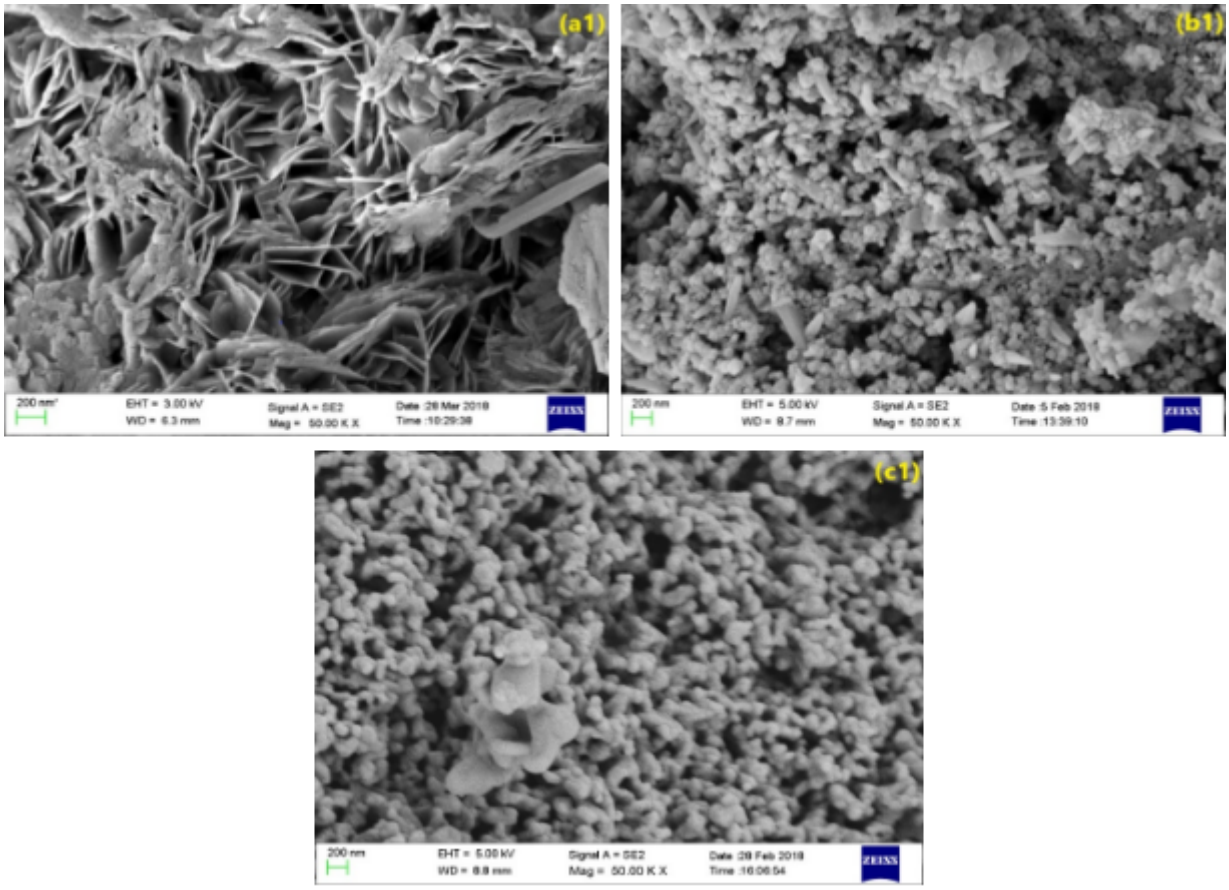

Figure 3

FESEM image of M doped BaFe2O4 nanoparticles with different metals such as (a1) for Cobalt, (b1) for Nickel and (c1) for Manganese.

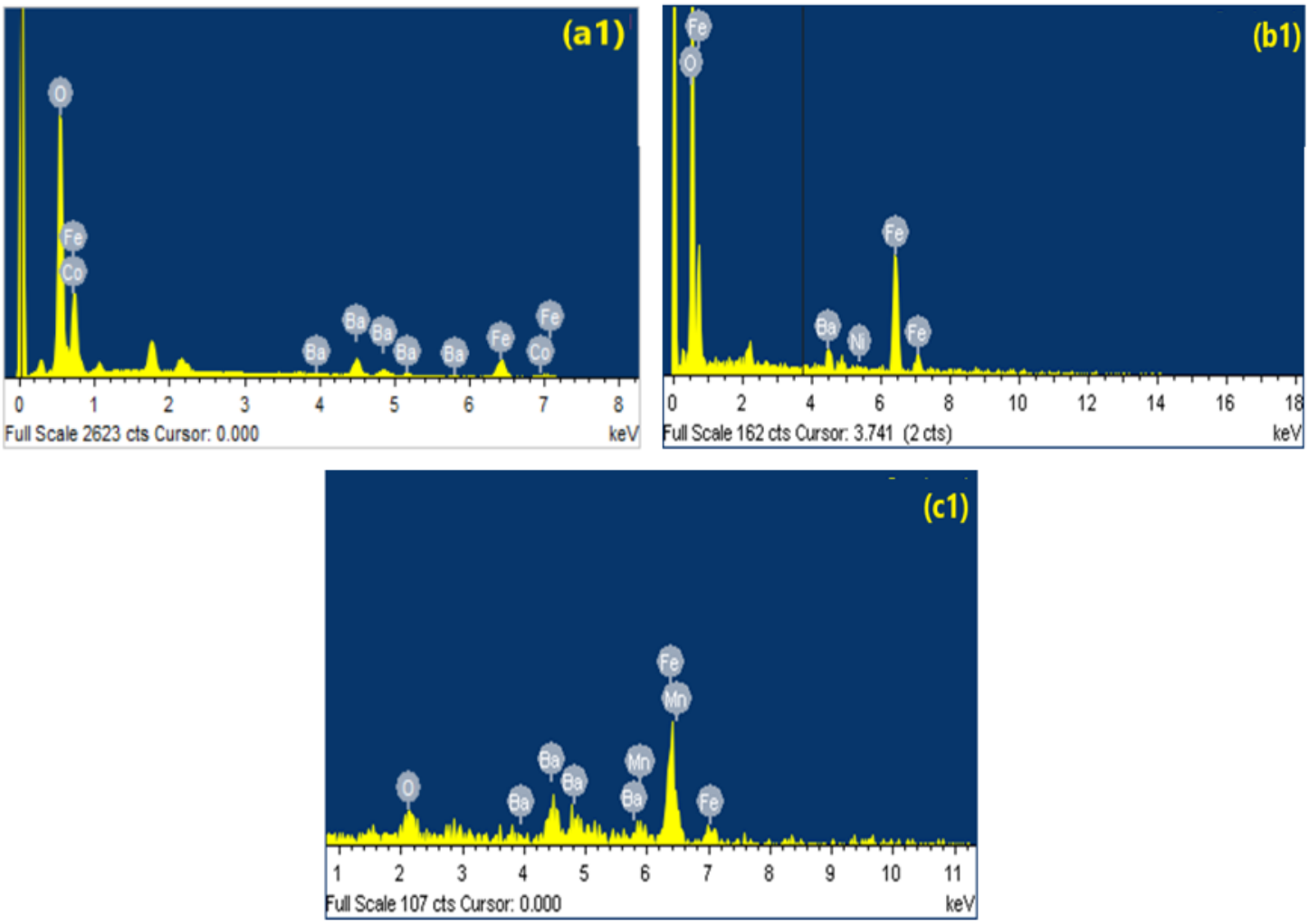

Figure 4

EDAX spectrum of M doped BaFe2O4 nanoparticles with different metals such as (a1) for Cobalt, (b1) for Nickel and (c1) for Manganese.

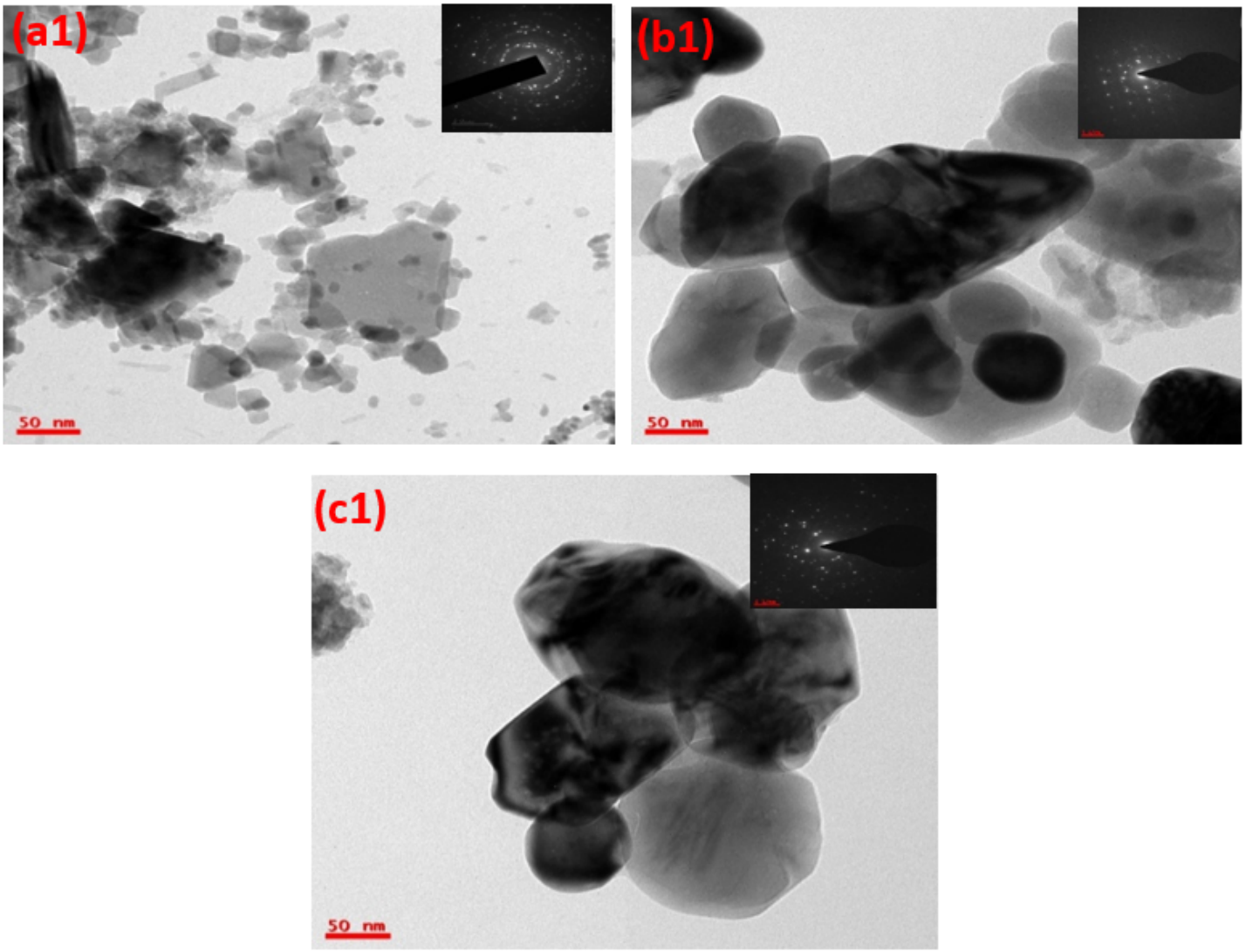

Figure 5

TEM images of M doped BaFe2O4 nanoparticles with different metals such as (a1) for Cobalt, (b1) for Nickel and (c1) for Manganese.

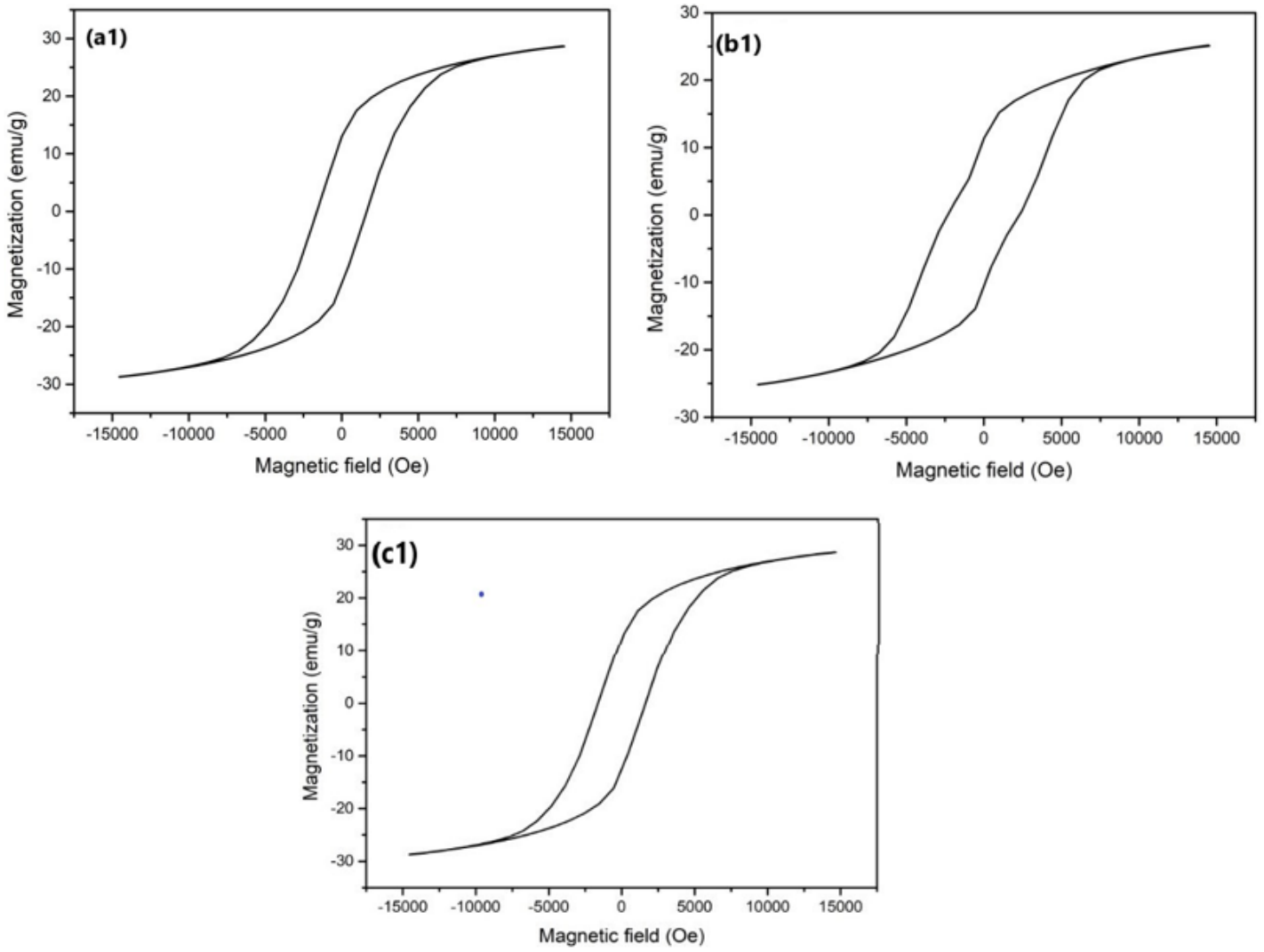

Figure 6

Hysteresis loop of M doped BaFe2O4 nanoparticles with different metals such as (a1) for Cobalt, (b1) for Nickel and (c1) for Manganese.

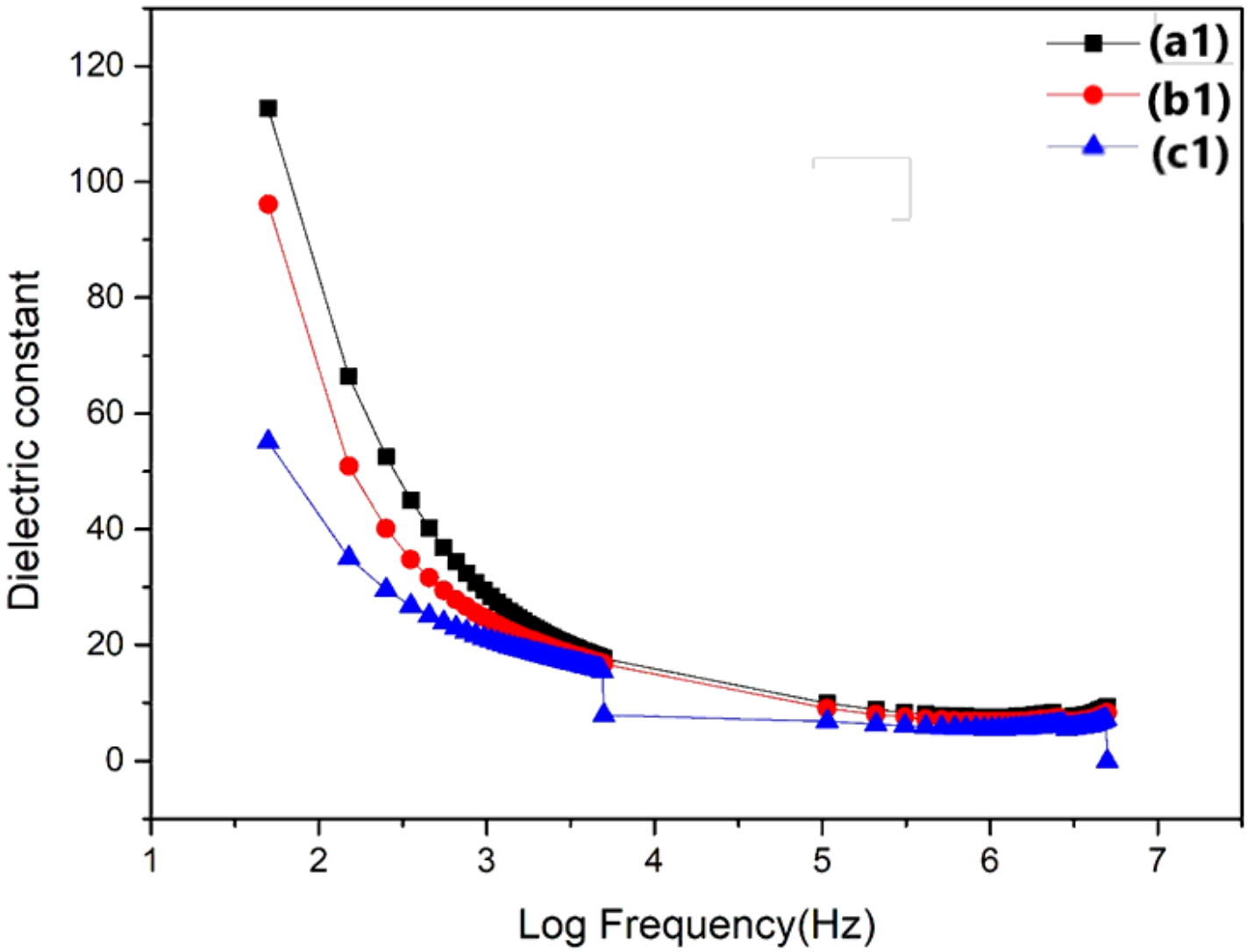

Figure 7

Dielectric constant of M doped BaFe2O4 nanoparticles with different metals such as (a1) for Cobalt, (b1) for Nickel and (c1) for Manganese.

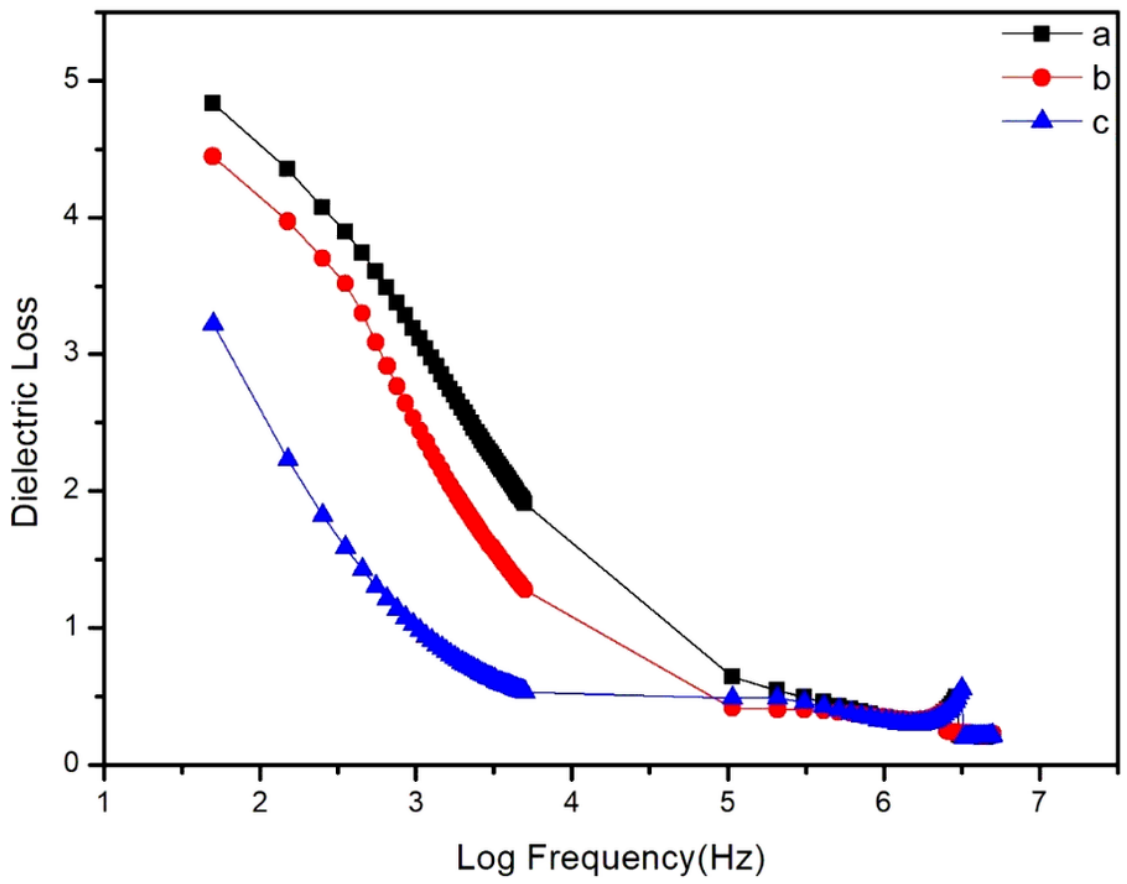

Figure 8

Dielectric loss of M doped BaFe2O4 nanoparticles with different metals such as (a) for Cobalt, (b) for Nickel and (c) for Manganese.